ELSEVIER

Biophysical Chemistry 126 (2007) 132–139

Biophysical Chemistry

http://www.elsevier.com/locate/biophyschem

An investigation of the ionic and solvation patterns of dsDNG versus dsDNA by use of molecular dynamics simulations

Joseph W. Toporowski, Swarnalatha Y. Reddy [1], Thomas C. Bruice *

Department of Chemistry and Biochemistry, University of California, Santa Barbara, CA 93106, United States

Received 4 February 2006; accepted 8 February 2006
Available online 9 March 2006

Abstract

Molecular dynamics has been employed to analyze the counterion and water atmospheres around the deoxynucleic guanidine (DNG) duplex $G_{12}{\cdot}C_{12}$. These features are compared to those of DNA $G_{12}{\cdot}C_{12}$. The chloride counterions of cationic DNG demonstrate fewer penetrations and only fleeting residence times in the minor groove, as opposed to the multi-nanosecond visits seen by sodium ions in DNA minor grooves. The 10 ns simulations also show the differences in hydration patterns between the DNG and DNA duplexes.

Keywords: Deoxynucleic guanadine; DNG; Molecular dynamics; DNA analogue; DNA ionic atmosphere; DNA hydration

1. Introduction

Deoxynucleic guanidine (DNG) is a positively charged DNA analogue in which the natural phosphate moiety is replaced with a guanidinium group (Fig. 1). By substituting the negatively charged phosphates of one duplex strand, not only is the electrostatic repulsion between the two strands eliminated (as is seen with neutral analogues such as peptide nucleic acids and methylphosphonates), but the opposite charges of a DNG·DNA duplex dramatically increases the stability compared to native dsDNA [1]. This laboratory has previously shown via synthetic, thermal denaturation, binding, and exonuclease studies that ssDNG binds to complementary ssDNA and RNA with high affinity and specificity, while being resistant to nuclease degradation [1–3]. The combination of these properties renders DNG an ideal candidate as a potential antisense/antigene agent.

Further studies of DNG have involved its self-association and the properties of dsDNG [1,4]. Understanding how DNG binds with itself addresses a fundamental property of the species which must be understood considering the species has potential in vivo applications. Furthermore, this laboratory has begun to investigate the potential of DNG in non-biological, material related fields, requiring a deeper comprehension of the complex's structural details. Initial spectral observations of complementary DNG hexamers in solution indicate the formation of DNG duplexes with melting temperatures below 5 °C (as is seen with DNA hexamers) [1]. Molecular dynamics (MD) has been employed to help examine the finer details of dsDNG oligomers. Previous 5 ns simulations [4] of DNG duplexes $d(Ag)_{12}{\cdot}d(Tg)_{12}$ and $d(Gg)_{12}{\cdot}d(Cg)_{12}$ suggest relatively straight, stiff B-DNA-like structures, properties which are thought to result from the greater rigidity of the sp^2 hybridized guanidinium backbone versus DNA's flexible sp^3 phosphate backbone. The dsDNG oligomers were also suggested to have the unique properties of deep minor grooves and very shallow major grooves, accompanied by large slide and *X*-displacement helical values.

Due to the polyionic nature of nucleic acids, their structural conformations, stability, and biological properties are heavily influenced by the surrounding solvent and ion atmosphere. While experimental techniques (X-ray crystallography, NMR) have revealed much about the intricacies of solvent and counterion effects on nucleic acids, MD has proven to be a powerful tool in augmenting these methods. MD has the ability to analyze time-dependant variables on an atomic scale and monitor trajectories of individual particles over multiple nanoseconds, making it well suited to examine such properties as the dynamic nature of solvent and counterions around DNA. The reliability and predictability of MD simulations has been markedly enhanced

* Corresponding author. Tel.: +1 805 893 2044; fax: +1 805 893 2229.
E-mail address: tcbruice@chem.ucsb.edu (T.C. Bruice).
[1] Current address: Invitrogen Molecular Probes, Eugene, OR 97402.

0301-4622/$ - see front matter © 2006 Elsevier B.V. All rights reserved.
doi:10.1016/j.bpc.2006.02.006

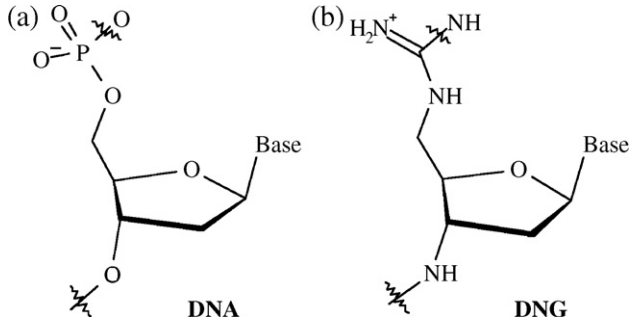

Fig. 1. Repeating unit of (a) DNA and (b) DNG.

with advances in computing power, force field development, and the treatment of long-range electrostatic interactions. Some limitations still exist though: a report from the Beveridge group demonstrates how ion motions are the rate-determining step in the total convergence of oligonucleotide simulations [5]. The report suggested that while the structural parameters of nucleic acids are stabilized within 3–5 ns of MD, ion convergence may take ≥100 ns, which is currently a computationally prohibitive timescale for most studies. Despite this slow ion convergence, numerous <10 ns MD reports have presented analyses of the counterion atmospheres around DNA [6–8]. So while the 10 ns simulations presented in this report may not achieve full ion convergence, a general view of the counterion activity around $G_{12}{\cdot}C_{12}$ dsDNG and dsDNA may be compared.

The true nature of the counterion atmosphere around DNA and the effects of counterions on DNA structure are topics currently under debate, and have been reviewed in detail in several recent articles [5,9,10]. X-ray crystallography studies have argued both for [11] and against [12] the presence of Na^+ in the minor grooves of A-tracts, however this technique is limited for this purpose by the difficulty in distinguishing between Na^+ ions and water molecules [13]. ^{23}Na NMR experiments have demonstrated a small presence (≤5%) of Na^+ in the minor grooves of A-tracts, with no related structural consequences [14]. The structural effects of ions proximal to DNA grooves remain unclear, though, with MD simulations both supporting [15] and opposing [5] the direct relationships of ion intrusion and groove width or axis bending, although the majority argue against such relationships. The counterion environment has been shown to be sequence dependant. Cations have been demonstrated to have a high propensity for the minor groove of A-tracts, while G-tracts have been shown to have cationic activity localized in the major grooves [11,16–18]. The overall view assembled from the collection of reports published to date are of a mobile Na^+ whose highest density lies around the phosphates, but has the ability to penetrate into the minor groove where it may stay for a period of time. However, the length of this residency varies, with reports of anywhere from 10 to 6000 ps. This report examines the counterion and solvent atmosphere around the DNG dodecamer $d(Gg)_{12}{\cdot}d(Cg)_{12}$ by use of 10 ns MD simulations, with the results compared to the DNA equivalent.

2. Methods

2.1. Setup

A detailed description of the DNG parameters, MD setup and execution, and structural analysis is given in a previous report [4]. The CHARMM27 all-atom nucleic acid residue topology and parameter files [19,20] were used for the DNA simulations, including counterions. The initial dodecamer structures were constructed using QUANTA98 [21], selecting B-DNA as an initial conformer. Counterions were added 5 Å from the phosphorous atoms of DNA or the guanidinium carbons of DNG to achieve neutral systems. These structures were energy minimized for 500 steps of steepest descent (SD) followed by 1000 steps of the adopted basis Newton–Raphson (ABNR) method using CHARMM (v. c27b4) [22].

2.2. MD details

The minimized systems were solvated in an orthorhombic box (44.7 × 64.0 × 43.7 Å) of pre-equilibrated TIP3P [23] water molecules, deleting those that had an oxygen atom within 2.8 Å of a solute heavy atom. Periodic boundary conditions were applied. Images were generated using the CRYSTAL module of CHARMM. Electrostatic interactions were treated with the particle mesh Ewald method [24,25], using a real space cutoff of 10 Å. The solvent was then minimized for 100 SD and 1000 ABNR steps while the solute was kept fixed. All constraints were then released and the entire system was minimized for 2000 ABNR steps. During dynamics, SHAKE [26] was used to constrain covalent bonds involving hydrogen atoms. The leapfrog-Verlet algorithm [27] was used for integration with a 1.5 fs time-step. The solute and counterions were initially constrained while the solvent was allowed to equilibrate at 300 K under constant pressure and temperature. The constraints on the ions were then released, followed by those on the

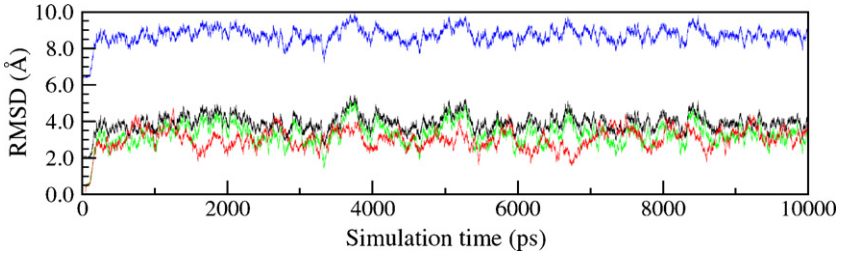

Fig. 2. RMSDs of non-terminal-residue DNG $G_{12}{\cdot}C_{12}$ atoms from B-DNA (black), A-DNA (blue), the minimized structure (green), and DNA $G_{12}{\cdot}C_{12}$ from the minimized structure (red). (For interpretation of the references to color in this figure legend, the reader is referred to the web version of this article.)

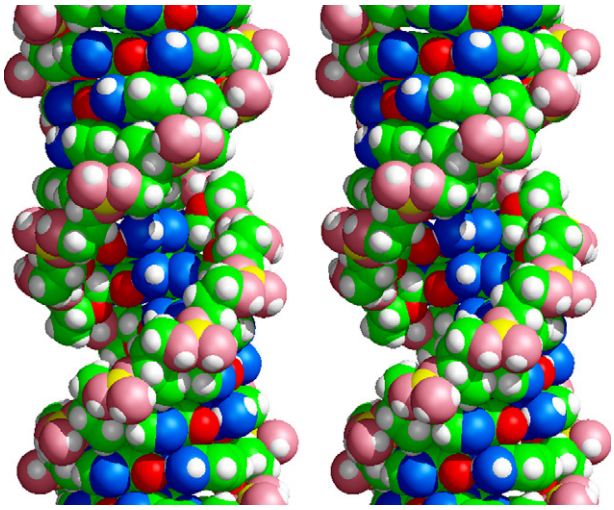

Fig. 3. Stereo view of 8–10 ns MD averaged DNG $G_{12}{\cdot}C_{12}$. To highlight the modified-DNA backbone, guanidinium carbons are shown in yellow and guanidinium nitrogens are colored pink. Note the especially shallow major groove and deep minor groove. (For interpretation of the references to colour in this figure legend, the reader is referred to the web version of this article.)

oligonucleotide, and the system was gradually heated to 300 K. After the total heating period of 135 ps, constant volume and temperature (NVT) conditions were invoked to achieve more stable trajectories [28], and the system continued to equilibrate for 365 ps. Following this initial 500 ps heating and equilibration period, the production stage was carried out using the NVT ensemble until the total dynamics time reached 10 ns.

2.3. Analyses

Root-mean-square deviations (rmsd) were evaluated by least-squares fitting to the minimized structures or canonical A or B forms, as noted, excluding the terminal base-pairs. Groove widths were defined as the distance between interstrand phosphorous atoms (or guanidinium carbons) separated by 3−4 base-pairs, i.e. P($i-2$)···P′($i+2$) across the major groove with four base-pair separation, and P′($i-2$)···P($i+2$) across the minor groove with three base-pair separation [29]. Average structures were obtained by a least squares fitting of all oligomer atoms saved at 0.75 ps intervals from the trajectories to the minimized structure. These averaged structures were minimized for 50 steps of SD, and the corresponding stereo plots were produced using MidasPlus [30,31]. The ion and water analyses were performed with the stand-alone version of *ptraj* (v.6.5) developed by Dr. Thomas Cheatham, which is capable of processing CHARMM trajectory files. This program was used to calculate the spatial distribution functions (SDFs) using 0.5 $Å^3$ grids over the entire simulation box, and binning atom positions from RMS coordinate fit frames at 0.75 ps intervals over the last 9 ns of the 10 ns simulations. Bulk water would then be expected to give 50.2 hits per grid over 9 ns, with the graphics presented here displaying water densities at 3.5 times that of bulk water and the ion densities shown at 7–12 hits per grid over 9 ns, as stated in the SDF captions. MidasPlus was used for contouring and to overlay the SDFs on the 1–10 ns averaged structures.

The electron density isosurface was evaluated by semiempirical molecular orbital calculations with PM3 parameters on the MD averaged (8–10 ns) central dimer base pairs of the G·C sequence using the program MOPAC2002 [32], incorporated in Fujitsu's CAChe software [33]. Solvent effects simulated by COSMO (Conductor-like Screening Model) were included. Electrostatic potential on the van der Waals surface was then generated by plotting electron density isosurface at 0.002 e/$Å^3$. The surface was colored to reflect the electrostatic potential at every point on the surface.

3. Results and discussion

3.1. RMSD

Analyses of the root mean square deviations (RMSD) for both the dsDNG and dsDNA $G_{12}{\cdot}C_{12}$ simulations show that stable

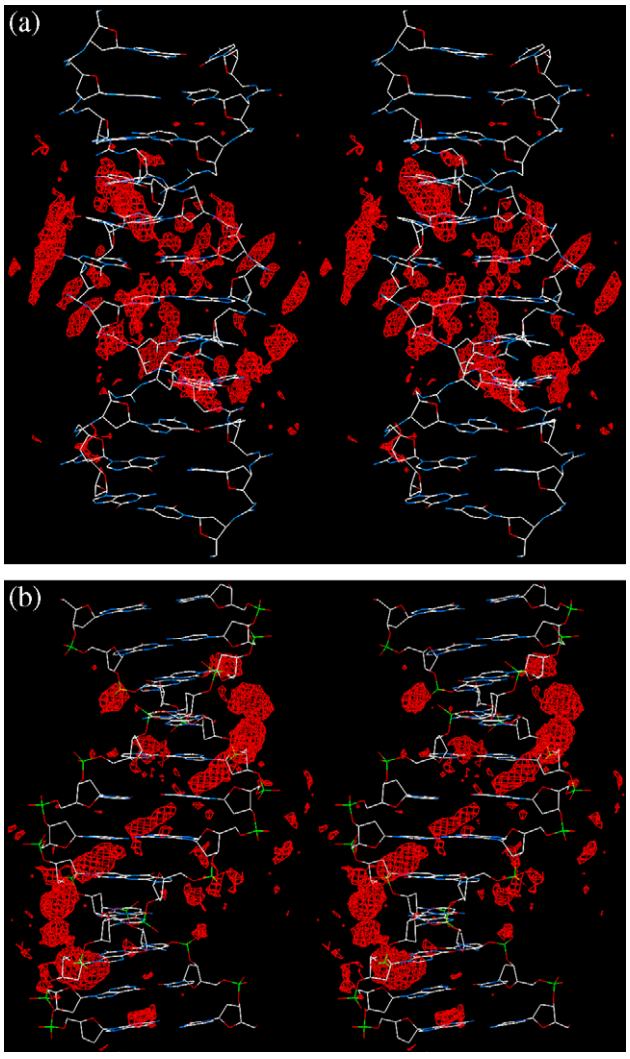

Fig. 4. Stereo views of the SDFs depicting regions of high counterion (red) concentrations around the MD averaged $G_{12}{\cdot}C_{12}$ structures: (a) DNG with Cl^- ions and (b) DNA with Na^+ ions. The contour levels represent regions of at least 7 ion counts per 1/2 $Å^3$ over the last 9 ns of MD. (For interpretation of the references to colour in this figure legend, the reader is referred to the web version of this article.)

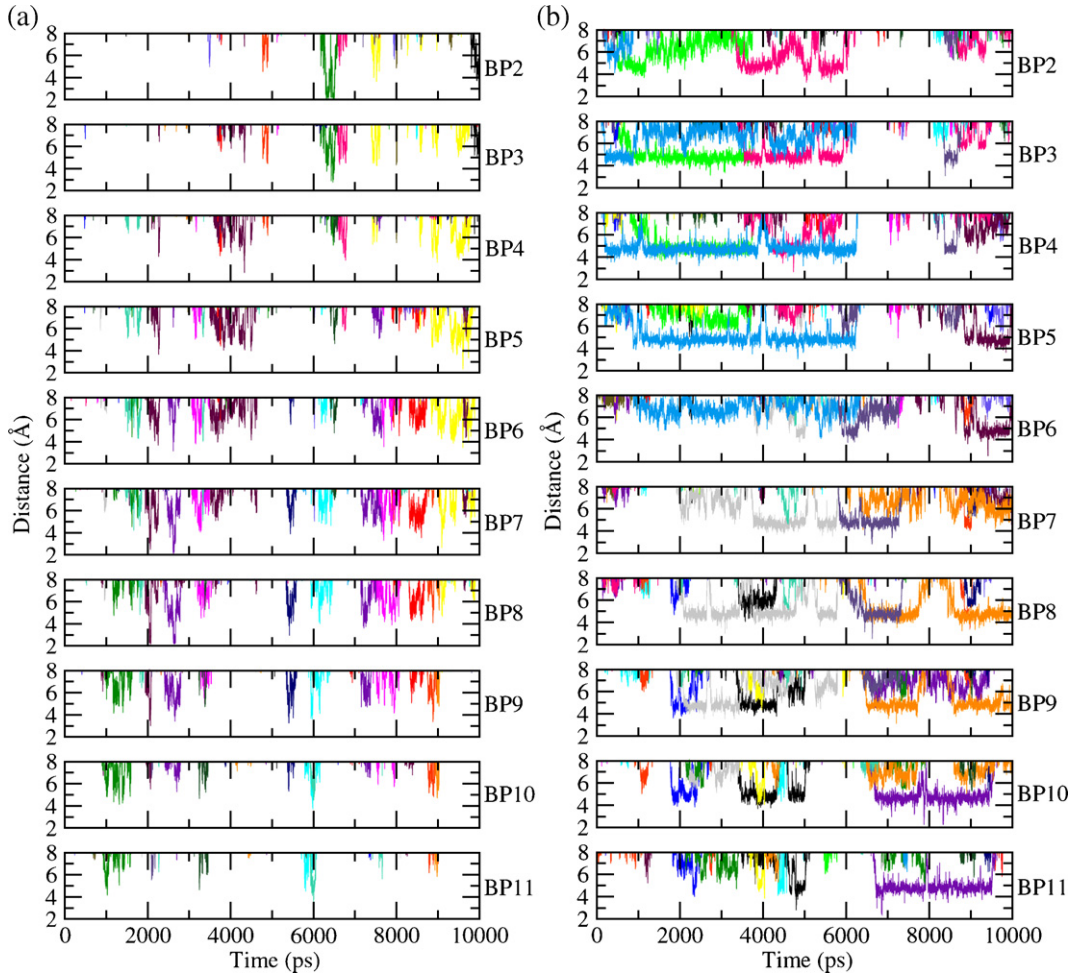

Fig. 5. Distances of counterions from their respective $d(G)_{12}\cdot d(C)_{12}$ minor groove binding partners: (a) Cl^- distances from guanine H22 of DNG, and (b) Na^+ distances from the closer of guanine N3 and cytosine O2 of DNA. Each color represents the trajectory of 1 of the 22 counterions per simulation. The central 10 base-pairs (BPs) are shown for both duplexes. Ions can often be seen to associate with 2 BPs simultaneously, represented by a single color appearing in adjacent graphs at similar distances during a particular time frame. (For interpretation of the references to colour in this figure legend, the reader is referred to the web version of this article.)

trajectories were achieved well within 500 ps (Fig. 2). The RMSD of DNG from B-DNA (3.9±0.5 Å, black) is much closer than from A-DNA (8.7±0.4 Å, blue). The RMSDs of both the DNG (green) and DNA (red) duplexes from their minimized structures are similar (3.3±0.6 and 3.0±0.6 Å, respectively). While the RMSDs suggest a DNG structure resembling B-DNA, it is the geometrical conformations which define the duplex as so.

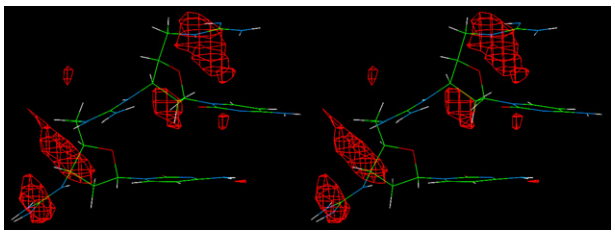

Fig. 6. Close-up stereo view of the SDF of Cl^- ions around the guanidinium functionality of the MD 1–10 ns averaged $G_{12}\cdot C_{12}$ DNG duplex, at a contour level representing 12 ion counts per 1/2 $Å^3$. This image of residues 5–7 of the poly-C strand shows a typical ion pattern found in the central part of the DNG duplex, with high ion concentration found on either side of the guanidinium NH_2 group.

3.2. Duplex structures

Similar to an earlier MD report [4], the modeled $d(Gg)_{12}\cdot d(Cg)_{12}$ duplex demonstrates a C2′-*endo* sugar pucker with helical parameters representative of a B-DNA structure, with

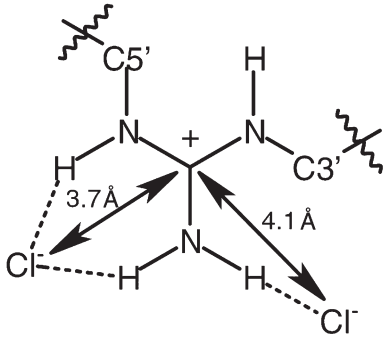

Fig. 7. Major conformations of Cl^- pairing with a guanidinium of DNG, along with distances from the guanidinium carbon. (The drawing is not meant to imply that two ions are bound simultaneously.)

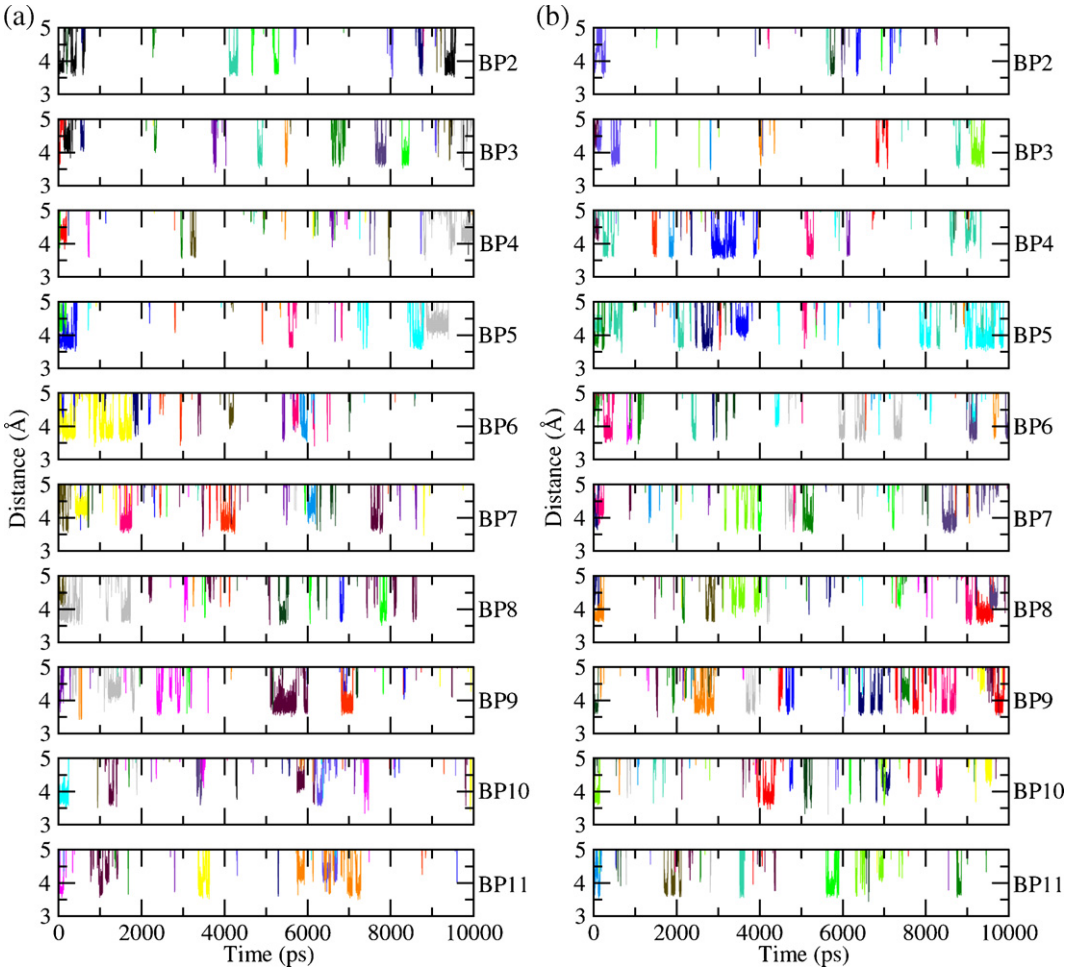

Fig. 8. Distances of 22 Cl^- counterions (each in a different color) from the guanidinium carbons of the central 10 base-pairs of (a) the guanine strand and (b) the cytosine strand of $d(Gg)_{12}{\cdot}d(Cg)_{12}$. (For interpretation of the references to colour in this figure legend, the reader is referred to the web version of this article.)

notably large slide, propeller, and X-displacement values. The minor groove of the duplex (13.1 ± 1.4 Å) is slightly narrower than that of the DNA counterpart (14.0 ± 1.1 Å), but the DNG model has an extremely shallow major groove and deep minor groove (Fig. 3).

3.3. Ion density distributions

Regions of high ion density around the $G_{12}{\cdot}C_{12}$ helices can be effectively visualized by use of spatial distribution functions (SDFs), as shown in Fig. 4. The SDFs show both similarities and

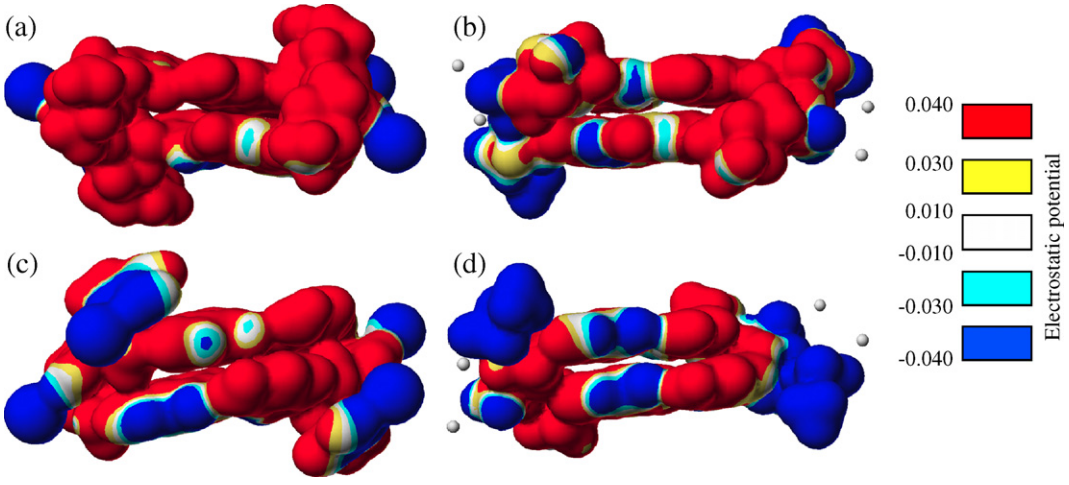

Fig. 9. ESP plots of $G_2{\cdot}C_2$ DNG (a,c) and DNA (b,d) dimers. Views are looking into the minor groove (a,b) and major groove (c,d).

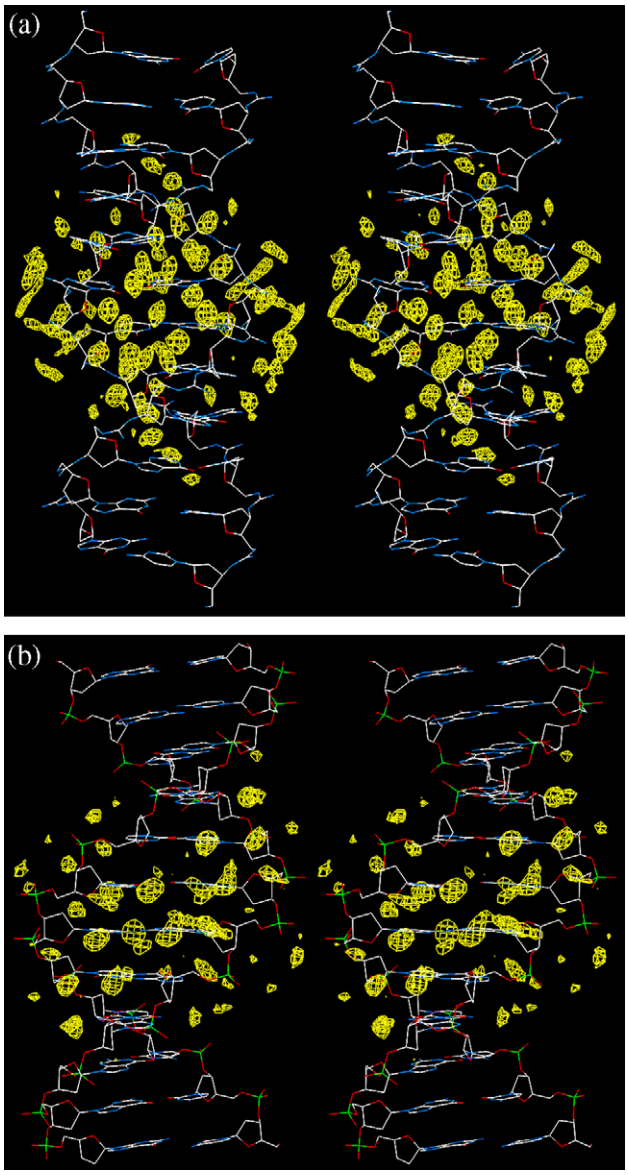

Fig. 10. Stereo views of the SDFs of water (yellow) around the MD 1–10 ns averaged $G_{12}{\cdot}C_{12}$ (a) DNG and (b) DNA structures. The contour levels represent 3.5× the density of bulk water. (For interpretation of the references to colour in this figure legend, the reader is referred to the web version of this article.)

differences in the counterion distribution between dsDNG and dsDNA. The Na^+ concentration around the DNA duplex is clearly most dense in the minor groove, with smaller high concentration regions located near some phosphates and in the major groove (Fig. 4b), supporting other MD studies of Na^+ in GC-rich sequences [10]. The Cl^- counterions of DNG can also be seen to take up residency in the minor groove, however the densest regions are limited to the central 8 base-pairs (Fig. 4a). High Cl^- concentration can also be found along the DNG backbone of these central 8 base-pairs. Na^+ ions have two electronegative atoms to potentially associate with in both the major groove (guanine O6 and N7) and minor groove (guanine N3 and cytosine O2), while Cl^- ions have one potential electron acceptor in both grooves: cytosine H41 in the major and guanine H22 in the minor.

While SDFs are ideal for viewing regions of high ion density, ion trajectories and residence times in the grooves can be nicely visualized with distances vs. time plots. Fig. 5 depicts the residence times of ions in the minor grooves of the dsDNG and dsDNA duplexes. While the Na^+ ions demonstrate a propensity to linger around the dsDNA minor groove electronegative atoms for periods ranging from 250 to 5000 ps (Fig. 5b), the dsDNG Cl^- ions are much more mobile and do not display interactions with their hydrogen electron acceptors lasting more than 200 ps (Fig. 5a). Besides the smaller ionic radius of the Na^+ versus Cl^-, the fact that Na^+ has two potential electronegative partners per base-pair in the minor groove surely increases the residence times. Simultaneous interactions of individual Na^+ or Cl^- ions with two base-pairs exist as well, as evidenced by single ions residing close to two base-pairs (Fig. 5).

As shown in Fig. 4a, the densest Cl^- regions lie around the guanidinium backbone. A more detailed view of the counterion environment is displayed in Fig. 6, a close-up stereo view, which depicts higher levels of ion density than Fig. 4a (contour level of 12 versus 7 ion counts per 1/2 $Å^3$). From this view, a region of high ion concentration can be seen on the 3′ side and in the same plane as the guanidinium group, with a larger region localized in the same plane but on the 5′ side of the group. These regions result from two possible ion pairing conformations, which are illustrated in Fig. 7. Cl^- associated on the 3′ end of the guanidinium forms a single hydrogen bond to the guanidinium NH_2 group. However on the 5′ side, the anion forms an additional hydrogen bond to the guanidinium hydrogen made available due to the conformation of the functional group. A similarly ordered ion pairing pattern was reported previously by Mason et al. in the MD study of guanidinium chloride solutions [34], with their reported ion–ion distances given in Fig. 7. The report also describes the lack of anions above and below the plane of unsubstituted guanidinium, a pattern also observed in the current study.

The trajectories of the Cl^- ions in close proximity to the DNG backbone are given in Fig. 8. Unlike the fleeting nature of the anions when forming brief hydrogen bonds in the minor groove (Fig. 5a), more substantial periods (up to 800 ps) of ion pairing to the guanidinium hydrogens are seen. During these times of ion pairing, the anions can be seen to assume one of two distinct distances from the guanidinium carbon (the difference between the two distances is well illustrated in BP5 of the guanine strand from ~8.5 to 9.5 ns, Fig. 8a). These distances average 3.7 and 4.1 Å, which represent both pairing conformations shown in Fig. 7. Similar patterns are seen in the cytosine strand (Fig. 8b).

3.4. Electron density surface

To aid in visualization of the charge distribution, electrostatic surface potential (ESP) maps of DNG and DNA G2·C2 dimers are given in Fig. 9. The most positive and negative regions of the surfaces are in red and blue, respectively. The dimers are based on the central base-pairs of MD averaged structures, with their respective counterions placed in high ion density regions: Cl^- ions 3.7 Å from the guanidinium carbons of DNG (as shown in Fig. 7), and Na^+ ions 3.2 Å away phosphate oxygens O1P and

O2P of DNA. The presence of the ions neutralizes the systems, reducing the extremes in magnitudes along the molecular surface. Not surprisingly, the most obvious differences between the ESPs of the dsDNG (Fig. 9a,c) and dsDNA (Fig. 9b,d) can be seen along the backbone. In addition to the greater positive charge of the DNG backbone, Cl^- ions can be seen to be encompassed by the electron density distribution, unlike the Na^+ ions of the DNA. The ESP inside the grooves (the nucleobases) is very similar between the DNG and DNA counterparts, although the electron-rich regions are more pronounced in the DNA. Electron-rich cytosine O2 and guanine N3 can be seen in the minor grooves in the bottom base-pair as cyan and blue in Fig. 9a (DNG) and 9b (DNA). Protruding from between these O2 and N3 atoms is electron-poor guanine H22 (red). In the major grooves (Fig. 9c,d), guanine N7 and O6 stand out as the primary electron-rich regions, while electropositive cytosine H41 can be seen to protrude on the opposite side of the groove. Altogether, the ESP maps reveal small (although protruding) regions available for Cl^- ion binding, compared to significantly larger electronegative regions available for Na^+ ion binding.

3.5. Solvent density distribution

The SDFs depicting the water environment around DNG and DNA are given in Fig. 10. Areas of well-ordered hydration can be seen in the DNA minor groove (Fig. 10b), where the water spine is comprised of two regions of high water density per base-pair located proximal to cytosine O2 and guanine N2 and N3 atoms, consistent with literature reports [35,36]. The deep DNG minor groove is shown to be highly hydrated (Fig. 10a). In addition to a central water spine on the floor of the minor groove, two dense regions on either side of the central spine can be seen proximal to cytosine O2 and guanine N2 and N3 atoms, similar to DNA. However, the guanidinium hydrogen which faces into the minor groove provides and extra opportunity for hydrogen bonding, increasing the overall hydration in the minor groove. High density water regions can also be seen around the DNG major groove, but because the groove is extremely shallow, the regions do not lie inside the groove. These hydration patterns support a previous MD study [4] on $G_{12}{\cdot}C_{12}$ and $A_{12}{\cdot}T_{12}$ DNG duplexes, in which the solvent-accessible surface areas (SASA) around the grooves and backbones were analyzed and compared to native DNA duplexes. The results showed higher hydration levels around the DNA phosphates compared to the DNG guanidiniums, while the DNG major grooves were substantially more hydrated than those of DNA, and the DNG and DNA minor grooves showed similar SASA. The ends of the duplexes in Fig. 10 appear to be less hydrated due to an artifact created when each snapshot is RMS fit to a common frame. Since the ends of the duplexes are more flexible, the density around these points appears lower, a point further discussed by Cheatham and Kollman [37].

4. Conclusion

We have reported here ion and solvation patterns of 10 ns simulations on dodecameric dsDNG and dsDNA $G_{12}{\cdot}C_{12}$ helices. Dense Na^+ ion patterns are observed in the minor groove of the DNA duplex, consistent with literature reports [7,10]. The densest Cl^- regions around the DNG helix are organized near the guanidinium groups, with ion activity also seen in the minor groove. The brief (<0.2 ns) residence times of Cl^- visits into the DNG minor groove are fleeting compared to the observed Na^+ ion penetrations into the DNA minor groove, which have residence times of 0.25−5.0 ns. This feature can be attributed to the two potential minor groove electronegative atoms available for Na^+ ions to associate with, as opposed to the single electron acceptor available for Cl^- ions. The ion binding patterns observed around the DNG backbone are in agreement with an MD study of guanidinium chloride solutions [37]. A central spine of hydration in the minor groove is the prominent solvent feature in both DNG and DNA helixes. In addition, DNG is characterized by dense hydration patterns on either side of this spine. Because of the shallowness and therefore increased accessibility of the DNG major groove, denser hydration patterns are observed here compared to the DNA major groove. Less hydration is observed around the DNG guanidiniums compared to DNA phosphates.

Acknowledgements

Support for this study has been provided by NIH grant 5R37DK09171.

References

[1] P.M. Reddy, T.C. Bruice, Solid-phase synthesis of positively charged deoxynucleic guanidine (DNG) oligonucleotide mixed sequences, Bioorg. Med. Chem. Lett. 13 (2003) 1281–1285.
[2] D.A. Barawkar, T.C. Bruice, Synthesis, biophysical properties, and nuclease resistance properties of mired backbone oligodeoxynucleotides containing cationic internucleoside guanidinium linkages: deoxynucleic guanidine/DNA chimeras, Proc. Natl. Acad. Sci. U. S. A. 95 (1998) 11047–11052.
[3] B.A. Linkletter, I.E. Szabo, T.C. Bruice, Solid-phase synthesis of deoxynucleic guanidine (DNG) oligomers and melting point and circular dichroism analysis of binding fidelity of octameric thymidyl oligomers with DNA oligomers, J. Am. Chem. Soc. 121 (1999) 3888–3896.
[4] J.W. Toporowski, S.Y. Reddy, T.C. Bruice, Comparison of positively charged DNG and DNA duplexes: a computational approach, Bioorg. Med. Chem. 13 (2005) 3691–3698.
[5] S.Y. Ponomarev, K.M. Thayer, D.L. Beveridge, Ion motions in molecular dynamics simulations on DNA, Proc. Natl. Acad. Sci. U. S. A. 101 (2004) 14771–14775.
[6] M. Feig, M. Pettitt, Sodium and chloride ions as part on the DNA solvation shell, Biophys. J. 77 (1999) 1769–1781.
[7] F. Mocci, G. Saba, Molecular dynamics simulations of A·T-rich oligomers: sequence specific binding of Na^+ in the minor groove of B-DNA, Biopolymers 68 (2003) 471–485.
[8] R. Stefl, J. Koca, Unrestrained molecular dynamics simulations of [d(AT)5]2 duplex in aqueous solution: hydration and binding of sodium ions in the minor groove, J. Am. Chem. Soc. 122 (2000) 5025–5033.
[9] M. Rueda, E. Cubero, C.A. Laughton, M. Orozco, Exploring the counterion atmosphere around DNA: what can be learned from molecular dynamics simulations? Biophys. J. 87 (2004) 800–811.
[10] P. Varnai, K. Zakrzewska, DNA and its counterions: a molecular dynamics study, Nucleic Acids Res. 32 (2004) 4269–4280.

[11] X. Shui, L. McFail-Isom, H.G.G., L.D. Williams, The B-DNA dodecamer at high resolution reveals a spine of water on sodium, Biochemistry 37 (1998) 8341–8355.
[12] T.K. Chiu, Kaczor-Grzeskowiak, R.E. Dickerson, Absence of minor groove monovalent cations in the crosslinked dodecamer C-G-C-G-A-A-T-T-C-G-C-G, J. Mol. Biol. 292 (1999) 589–608.
[13] V. Tereshko, C.J. Wilds, G. Minasov, T.P. Prakash, M.A. Maier, A. Howard, Z. Wawrzak, M. Manoharan, M. Egli, Detection of alkali metal ions in DNA crystals using state-of-the-art X-ray diffraction experiments, Nucleic Acids Res. 29 (2001) 1208–1215.
[14] V.P. Denisov, B. Halle, Sequence-specific binding of counterions to B-DNA, Proc. Natl. Acad. Sci. U. S. A. 97 (2000) 629–633.
[15] D. Hamelberg, L. McFail-Isom, L.D. Williams, W.D. Wilson, Flexible structure of DNA: ion dependence of minor-groove structure and dynamics, J. Am. Chem. Soc. 122 (2000) 10513–10520.
[16] M. Egli, DNA–cation interactions: quo vadis? Chem. Biol. 9 (2002) 277–286.
[17] N.V. Hud, M. Polak, DNA–cation interactions: the major and minor grooves are flexible ionophores, Curr. Opin. Struct. Biol. 11 (2001) 293–301.
[18] N.V. Hud, V. Sklenar, J. Feigon, Localization of ammonium ions in the minor groove of DNA duplexes in solution and the origin on DNA A-tract bending, J. Mol. Biol. 286 (1999) 651–660.
[19] A.D. MacKerell Jr., D. Bashford, M. Bellott, R.L. Dunbrack, J.D. Evanseck, M.J. Field, S. Fischer, J. Gao, H. Guo, S. Ha, D. Joseph-McCarthy, L. Kuchnir, K. Kuczera, F.T.K. Lau, C. Mattos, S. Michnick, T. Ngo, D.T. Nguyen, B. Prodhom, W.E. Reiher, B. Roux, M. Schlenkrich, J.C. Smith, R. Stote, J. Straub, M. Watanabe, J. Wiórkiewicz-Kuczera, D. Yin, M. Karplus, All-atom empirical potential for molecular modeling and dynamics studies of proteins, J. Phys. Chem., B 102 (1998) 3586–3616.
[20] A.D. MacKerell, N. Banavali, All-atom empirical force field for nucleic acids. II. Application to molecular dynamics simulations of DNA and RNA in solution, J. Comput. Chem. 21 (2000) 105–120.
[21] QUANTA98, Molecular Simulation Inc. (1998) San Diego, CA.
[22] B.R. Brooks, R.E. Bruccoleri, B.D. Olafson, D.J. States, S. Swaminathan, M. Karplus, CHARMM: a program for macromolecular energy, minimization, and dynamics calculations, J. Comput. Chem. 4 (1983) 187–217.
[23] W.L. Jorgensen, J. Chandrasekhar, J.D. Madura, R.W. Impey, M.L. Klein, Comparison of simple potential functions for simulating liquid water, J. Chem. Phys. 79 (1983) 926–935.
[24] T. Darden, D. York, L. Pedersen, Particle mesh Ewald: an N∗log(N) method for Ewald sums in large systems, J. Chem. Phys. 98 (1993) 10089–10092.
[25] H.G. Petersen, Accuracy and efficiency of the particle mesh Ewald method, J. Chem. Phys. 103 (1995) 3668–3679.
[26] J.P. Ryckaert, G. Ciccotti, H.J.C. Berendsen, Numerical integration of the Cartesian equations of motion of a system with constraints: molecular dynamics of n-alkanes, J. Comput. Phys. 23 (1977) 237–241.
[27] L. Verlet, Computer "experiments" on classical fluids. I. Thermodynamical properties of Lennard–Jones molecules, Phys. Rev. 159 (1967) 98–103.
[28] D. Brown, J.H.R. Clarke, A comparison of constant energy, constant temperature and constant pressure ensembles in molecular-dynamics simulations of atomic liquids, Mol. Phys. 51 (1984) 1243–1252.
[29] K.M. Kosikov, A.A. Gorin, X.-J. Lu, W.K. Olson, G.S. Manning, Bending of DNA by asymmetric charge neutralization: all-atom energy simulations, J. Am. Chem. Soc. 124 (2002) 4838–4847.
[30] T.E. Ferrin, C.C. Huang, L.E. Jarvis, R. Langridge, The Midas Display System, J. Mol. Graph. 6 (1988) 13–27.
[31] C.C. Huang, E.F. Pettersen, T.E. Klein, T.E. Ferrin, R. Langridge, Conic — a fast renderer for space-filling molecules with shadows, J. Mol. Graph. 9 (1991) 230–236.
[32] J.J.P. Stewart, Optimization of parameters for semiempirical methods I. Method, J. Comput. Chem. 10 (1989) 209–220.
[33] CAChe 6.1, Computer Aided Chemistry software, Fujitsu limited.
[34] P.E. Mason, G.W. Neilson, J.E. Enderby, M.-L. Saboungi, C.E. Dempsey, A.D. MacKerell Jr., J.W. Brady, The structure of aqueous guanidinium chloride solutions, J. Am. Chem. Soc. 126 (2004) 11462–11470.
[35] S.Y. Reddy, F. Leclerc, M. Karplus, DNA polymorphism: a comparison of force fields for nucleic acids, Biophys. J. 84 (2003) 1421–1449.
[36] V. Tereshko, G. Minasov, M. Egli, A "hydrat-ion" spine in a B-DNA minor groove, J. Am. Chem. Soc. 121 (1999) 3590–3595.
[37] T.E.I. Cheatham, P.A. Kollman, Molecular dynamics simulations highlight the structural differences among DNA:DNA, RNA:RNA, and DNA:RNA hybrid duplexes, J. Am. Chem. Soc. 119 (1997) 4805–4825.